International Journal of Minerals, Metallurgy and Materials
Volume 19, Number 8, Aug 2012, Page 747
DOI: 10.1007/s12613-012-0622-2

Eutectic reaction and cored dendritic morphology in yttrium doped Zr-based amorphous alloys

Wei-jie Peng and Yong Zhang

State Key Laboratory for Advanced Metals and Materials, University of Science and Technology Beijing, 100083, China

(Received: 4 July 2011; revised: 9 July 2011; accepted: 5 September 2011)

Abstract: The microalloying effect of yttrium on the crystallization behaviors of $(Zr_{0.525}Al_{0.10}Ti_{0.05}Cu_{0.179}Ni_{0.146})_{100-x}Y_x$, and $(Zr_{0.55}Al_{0.15}Ni_{0.10}Cu_{0.20})_{100-x}Y_x$ (x=0, 0.4, and 1, thus the two alloy systems were denoted as Zr52.5, Zr52.5Y0.4, Zr52.5Y1, and Zr55, Zr55Y0.4, Zr55Y1, respectively) was studied. Transmission electron microscopy (TEM) results suggested that the crystalline phases were different in the two Zr-based alloys and with different yttrium contents. ZrNi-phase and Al_3Zr_5 phase precipitations can be well explained by the mechanisms of nucleation and growth. Al_3Zr_5 phase is mainly formed by a peritectic-like reaction, while ZrNi-phase by a eutectic reaction. The contents of elements Y, Al, and Ti may dominate the reaction types. The orientation relationship between Y_2O_3 particles and Al_3Zr_5 phase is also discussed.

Keywords: zirconium alloys; amorphous alloys; bulk metallic glasses; yttrium; eutectic structure; dendritic structure

1. Introduction

The formation of amorphous phases is directly related to the suppression of nucleation and growth of crystalline phases. By studying the crystallization behavior, the ways for the stabilization of amorphous phases and the increase of glass formability (GFA) can be revealed.

The crystallization behavior of Zr-based metallic glasses has been studied extensively. Moreover, a series of crystalline phases have been reported and discussed for Zr-based metallic glasses [1-7]. There are many factors to affect the crystallization behaviors and the glass formation mechanism [8-10], e.g., cooling rates [11], material purities [1, 12], mixing entropy, and atomic packing efficiency [1-6, 11]. In these factors, composition variation plays an important role. Crystalline phases are very sensitive to alloy compositions.

Minor addition is a useful way to adjust alloy compositions [3, 13-16]. It is widely recognized that yttrium is one of the magic minor addition elements for scavenging oxygen impurity, adjusting composition closer to eutectic, and suppressing primary Zr_4Ni_2O phase formation [15, 17-19]. In this work, yttrium was selected to study nucleation and growth of crystalline phases in $Zr_{52.5}Al_{10}Ti_5Cu_{17.9}Ni_{14.6}$ and $Zr_{55}Al_{15}Ni_{10}Cu_{20}$ alloys from different perspectives.

2. Experimental

Zr-based alloy ingots with compositions of $(Zr_{0.525}Al_{0.10}Ti_{0.05}Cu_{0.179}Ni_{0.146})_{100-x}Y_x$ and $(Zr_{0.55}Al_{0.15}Ni_{0.10}Cu_{0.20})_{99}Y_x$ (x=0, 0.4, 1) were prepared by arc melting the mixture of pure Zr, Ni, Cu, Al, Ti, and Y in an argon atmosphere. Each ingot was melted at least three times to obtain chemical homogeneity. Then, these ingots were cast by copper mold suction casting method to obtain rod samples of 5 mm in diameter. The structure of these alloys was observed by transmission electron microscopy (TEM).

3. Results

TEM images of Zr-based alloys, as shown in Fig. 1, reveal the microstructure evolution with alloy composition variation. Fig. 1(a) shows morphologies of the amorphous matrix and two crystals in a Zr52.5Y0.4 rod sample: one is Y_2O_3 phase, which has been identified as a BCC structure

Corresponding author: Wei-jie Peng E-mail: pwjxfys@163.com

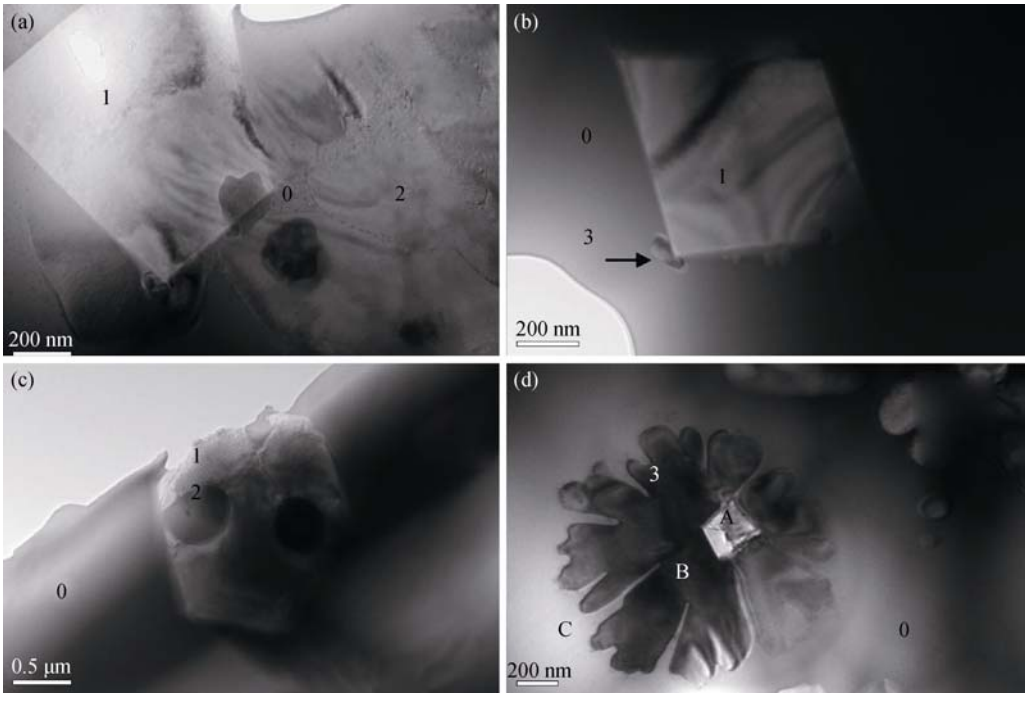

Fig. 1. TEM images of Zr52.5Y0.4 (a), Zr52.5Y1 (b), Zr55Y0.4 (c), and Zr55Y1 (d) alloys (in the figure, 1—Y_2O_3 phase, 2—ZrNi-phase, 3—Al_3Zr_5 phase, 0—amorphous, and the compositions of points A, B, and C have been given in Table 1).

crystal with lattice parameter a=1.05 nm; and the other is a bulk crystal, which is an FCC structure with lattice parameter a=1.40 nm. Energy dispersive spectrometry (EDS) analysis indicates that the composition of the bulk crystal is mainly Zr and Ni (ZrNi-phase).

In Zr55Y0.4 alloy, Y_2O_3 phase and ZrNi-phase can also be observed, although their morphologies (Fig. 1(c)) are different from those in Zr52.5Y0.4 alloy.

When the yttrium content reaches 1at%, the mainly precipitated phase in Zr52.5 alloy is still ZrNi-phase. However, (Zr,Al)-rich phase bean-shaped particles, as shown in Fig. 1(b), can be found. The size of the bean-shaped phase is just several microns, and its composition is similar to that of dendrite phase in Zr55Y1 alloy (Fig. 1(d)). Electron diffraction (Fig. 2) result suggests that the dendrite phase is a hexagonal structure with lattice parameter a=0.89 nm, which is consistent with Al_3Zr_5 phase.

Fig. 2 shows an orientation relationship between Al_3Zr_5 phase and Y_2O_3 phase: $(20\bar{2}\bar{1})$ Al_3Zr_5 ∥ $(01\bar{1})$ Y_2O_3. This indicates a low interfacial energy and small misfit between Al_3Zr_5 and Y_2O_3 phases.

Fig. 3 shows the X-ray diffraction patterns of Zr52.5Y0.4, Zr52.5Y1, Zr55Y0.4, and Zr55Y1 alloys. The results indicate that ZrNi-phase is the main precipitated phase of Zr52.5Y0.4 alloy. With the increase of Y addition from 0.4at% to 1at%, the XRD results show that Zr52.5 alloy is more sensitive and effective to yttrium addition.

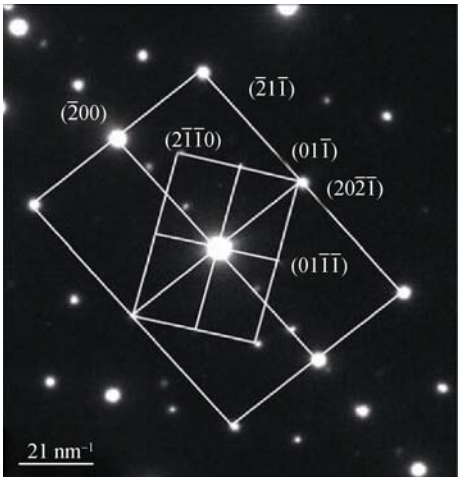

Fig. 2. Electron diffraction patterns of Y_2O_3 and Al_3Zr_5 phases.

For Zr55Y0.4 alloy, the mainly precipitated phase is still ZrNi-phase. However, the XRD peaks suggest the existence of Al_3Zr_5 phase in Zr55Y1 alloy. These results are consistent with TEM microstructure analyses. Fig. 4 presents the differential scanning calorimetry (DSC) curves of Zr52.5Y0, Zr52.5Y0.4, Zr55Y0.4, and Zr55Y1 alloys. All the curves show an endothermic inflection point because of the glass transition followed by the supercooled liquid region and

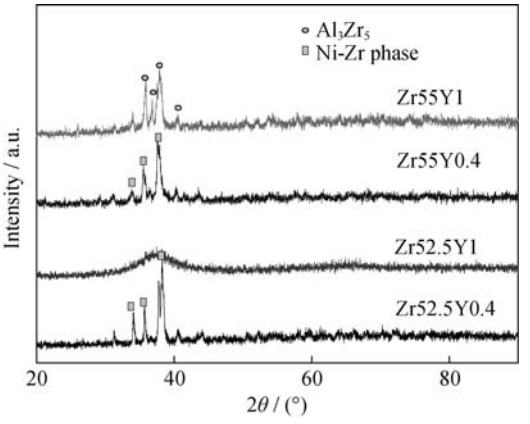

Fig. 3. XRD patterns obtained from Zr52.5Y0.4, Zr52.5Y1, Zr55Y0.4, and Zr55Y1 alloy rod samples.

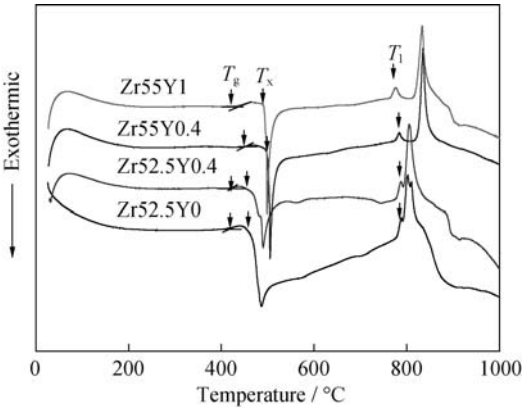

Fig. 4. DSC traces obtained from Zr52.5Y0, Zr52.5Y0.4, Zr55Y0.4, and Zr55Y1 ribbons.

then exothermic reactions because of the crystallization of amorphous phases. Zr55Y1 alloy has lower T_g than Zr55Y0.4 alloy. However, the changes of T_g and T_l are not apparent with yttrium addition.

4. Discussion

The different crystallization behaviors of the two alloy systems, e.g., the size and morphology of the crystalline phases, ZrNi-phase, and Al_3Zr_5 phase, and their orientation relationship with Y_2O_3 phase, indicate that the nucleation and growth mechanisms are different for these two phases.

The possible mechanisms are sketched diagrammatically in Fig. 5. For ZrNi-phase, the eutectic reaction may be explained to be the dominant mechanism:

$L \rightarrow Y_2O_3 + ZrNi\text{-phase}$

During quenching, Y_2O_3 phase and ZrNi-phase precipitate from liquid. Usually, in the eutectic reaction, it takes some time after the nucleation of two phases for them to establish cooperation and growth in the well-known eutectic fashion. However, in a copper mold suction casting method, there is insufficient time for coupled growth to be established. The resulting microstructures of the eutectic reaction, in which Y_2O_3 phase and ZrNi-phase have not been able to establish cooperation, are coarser and are often called a degenerate eutectic structure (as shown in Fig. 1(a)). A little amorphous phase retains in the interface between Y_2O_3 phase and ZrNi-phase.

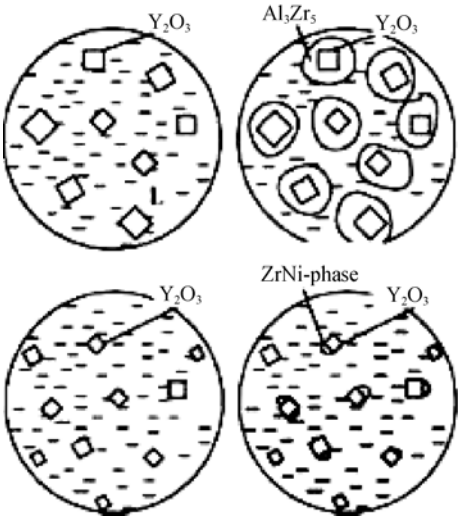

Fig. 5. Sketch of phase precipitation in yttrium doped Zr-based alloys.

In previous work, it was reported that Y_2O_3 could react with Zr55 alloy to form a white phase, and EDS analysis indicated that the composition of the white phase was 8.4at% Al, 11.16at% Cu, 26.27at% Zr, 9.32at% Y, 39.82at% O, and 4.96at% Ni. The reaction can be expressed by $L + Y_2O_3 \rightarrow$ white phase [19].

However, in this work, the white phase has not been found. Although Al_3Zr_5 phase indicates a cored dendritic morphology (as shown in Fig. 1(d)), its composition is different from that of the white phase.

The formation of Al_3Zr_5 phase can be explained by the peritectic-like reaction. In the peritectic-like reaction, Y_2O_3 phase precipitates as a primary phase, and after that Al_3Zr_5 phase forms. Y_2O_3 phase is a good nucleant for Al_3Zr_5 phase and may supply purity heterogeneous nucleation interfaces. Al_3Zr_5 phase will form with a strong tendency to grow around Y_2O_3 phase, then, the cored dendritic morphology can be observed.

The precipitations of ZrNi-phase and Al_3Zr_5 phase depend greatly on yttrium content. In the alloy containing 0.4at% yttrium, almost all of the yttrium elements are associated with oxygen to form Y_2O_3 particles. It is difficult to

find yttrium element in the amorphous matrix.

However, in Zr55Y1 alloy, a few yttrium contents have been detected in the matrix. The compositions of three points in Fig. 1(d) are given in Table 1. Amorphous alloys are very sensitive to compositions. It can be assumed that alloy composition, mainly Al, Ti, and Y components in the matrix, can influence crystal precipitation in Zr-based amorphous alloys [20-23]. The higher Al content and lower Ti content may lead to the easier precipitation of Al_3Zr_5 phase.

Table 1. Crystal phases and compositions in Fig. 1(d)

Point	Crystal structure	Lattice parameter, a / nm	Composition /at%						
			Zr	Al	Ni	Cu	Ti	Y	O
A	BCC	1.05	3.75	1.27	0.87	3.81	0	58.39	31.91
B	HCP	1.70	56.32	27.87	1.01	14.79	—	0	—
C	—	—	50.82	10.07	13.53	25.09	—	0.49	—

According to the empirical electron theory of solids (EET) and molecules [24], the number of electron pairs (n_c) of Zr-Al and Ti-Al atomic groups can be estimated. The relationship between bond length ($D_{(n_c)}^{u-v}$) and n_c can be expressed as

$$D_{(n_c)}^{u-v} = R^u + R^v - \beta \lg n_c ,$$

where u and v are the bonding atoms, R^u and R^v are the half-single bond distances, and β is a parameter. In the Zr-Al group, the value of n_c is about 0.341, which is lower than 0.399 in Ti-Al groups.

In view of the difference of atomic arrangement between amorphous phases and crystals, the value of n_c is inaccuracy, although it indeed indicates a strong bond between Al and Ti atoms. The presence of Ti can suppress the precipitation of Al_3Zr_5 phase in 0.4at% yttrium-containing alloys. With increasing yttrium content, redundant yttrium atoms may change a liquidus structure. Therefore, Al_3Zr_5 phase forms.

5. Conclusions

In Zr-based alloys, precipitation phases are very sensitive to alloy composition. With composition variation, especially the changes of Al, Ti, and Y contents, two formation mechanisms dominate the precipitation process: eutectic reaction and peritectic-like reaction.

In this work, the increase of yttrium content would result in a transition from the eutectic to peritectic-like reaction. Moreover, the precipitated phases are changed.

The eutectic reaction can lead to the precipitation of ZrNi-phase. The reaction mechanism can be expressed as $L \rightarrow Y_2O_3$+ZrNi-phase.

The precipitation mechanism for Al_3Zr_5 phase with the cored dendritic morphology can be explained by the peritectic-like reaction. In the peritectic-like reaction, Y_2O_3 phase precipitates as a primary phase, and after that Al_3Zr_5 phase forms. There is an orientation relationship between Y_2O_3 phase and Al_3Zr_5 phase: $(20\bar{2}\bar{1})$ $Al_3Zr_5 \parallel (01\bar{1})$ Y_2O_3. Y_2O_3 phase can act as heterogeneous nucleation for Al_3Zr_5 phase.

References

[1] Y. Zhang, M.X. Pan, D.Q. Zhao, R.J. Wang, and W.H. Wang, Formation of Zr-based bulk metallic glasses from low purity of materials by yttrium addition, *Mater. Trans.*, 41(2000), No.11, p.1410.

[2] C.T. Liu, M.F. Chisholm, and M.K. Miller, Oxygen impurity and microalloying effect in a Zr-based bulk metallic glass alloy, *Intermetallics*, 10(2002), No.11-12, p.1105.

[3] J.B. Qiang, W. Zhang, and A. Inoue, Formation and compression mechanical properties of Ni-Zr-Nb-Pd bulk metallic glasses, *J. Mater. Res.*, 23(2008), No.7, p.1940.

[4] Q. Jing, Y. Zhang, D. Wang, and Y. Li, A study of the glass forming ability in ZrNiAl alloys, *Mater. Sci. Eng. A*, 441(2006), No.1-2, p.106.

[5] Y.J. Sun, D.D. Qu, Y.J. Huang, K.D. Liss, X.S. Wei, D.W. Xing, and J. Shen, Zr-Cu-Ni-Al bulk metallic glasses with superhigh glass-forming ability, *Acta Mater.*, 57(2009), No.4, p.1290.

[6] Z.J. Yan, J.F. Li, S.R. He, and Y.H. Zhou, Relation between formation of compounds and glass forming ability for Zr-Al-Ni alloys, *Mater. Lett.*, 57(2003), No.12, p.1840.

[7] X.D. Wang, H. Lee, and S. Yi, Crystallization behavior of preannealed bulk amorphous alloy $Zr_{62}Al_8Ni_{13}Cu_{17}$, *Mater. Lett.*, 60(2006), No.7, p.935.

[8] N.H. Tariq, B.A. Hasan, and J.I. Akhter, Evolution of microstructure in $Zr_{55}Cu_{30}Al_{10}Ni_5$ bulk amorphous alloy by high power pulsed Nd:YAG laser, *J. Alloys Compd.*, 485(2009), No.1-2, p.212.

[9] D. Xing, J. Shen, L. Zhang, J. Sun, X. Wang, Y. Huang, and P.K. Liaw, Evolution of the primary crystals and the amor-

phous matrix following annealing of a bulk $Zr_{56.6}Cu_{17.3}Ni_{12.5}Al_{9.6}Ti_4$ metallic glass, *Mater. Sci. Eng. A*, 513-514(2009), p.8.

[10] P.N. Zhang, J.F. Li, Y. Hu, Y.H. Zhou, Microstructural evolution during annealing and rolling $Zr_{52.5}Cu_{17.9}Ni_{14.6}Al_{10}Ti_5$ bulk metallic glass, *Mater. Sci. Eng. A*, 499(2009), No.1-2, p.374.

[11] C.W. Kim, H.G. Jeong, and D.B. Lee, Oxidation of $Zr_{65}Al_{10}Ni_{10}Cu_{15}$ bulk metallic glass, *Mater. Lett.*, 62(2008), No.4-5, p.584.

[12] D. Xing, J. Shen, L. Zhang, J. Sun, X. Wang, H. Wang, Y. Huang, and P.K. Liaw, Investigation of precipitation phases in as-cast wedge ingot of bulk amorphous $Zr_{56.6}Cu_{17.3}Ni_{12.5}Al_{9.6}Ti_4$ alloy, *J. Alloys Compd.*, 481(2009), No.1-2, p.531.

[13] F. Chen, M. Takagi, T. Imura, Y. Kawamura, H. Kato, and A. Inoue, Crystallization of $Zr_{55}Al_{10}Ni_5Cu_{30}$ bulk metallic glass composites containing ZrC particles, *Mater. Trans.*, 43(2002), No.1, p.1.

[14] M. Ishikuro and K. Wagatsuma, Separation and determination of zirconium carbide in $Zr_{50}Al_{10}Ni_5Cu_{30}$ bulk metallic glass matrix composites containing ZrC particles, *Mater. Trans.*, 51(2010), No.2, p.366.

[15] C.T. Liu and Z.P. Lu, Effect of minor alloying additions on glass formation in bulk metallic glasses, *Intermetallics*, 13(2005), No.3-4, p.415.

[16] W.H. Wang, Roles of minor additions in formation and properties of bulk metallic glasses, *Prog. Mater. Sci.*, 52(2007), No.4, p.540.

[17] H.J. Wang, G.J. Shiflet, S.J. Poon, K. Matsuda, and S. Ikeno, The role of Y/lanthanides on the glass forming ability of amorphous steel, *Appl. Phys. Lett.*, 91(2007), No.14, art. no.141910.

[18] Z.P. Lu and C.T. Liu, Role of minor alloying additions in formation of bulk metallic glasses: a review, *J. Mater. Sci.*, 39(2004), No.12, p.3965.

[19] W.J. Peng and Y. Zhang, Micro-alloying of yttrium in Zr-based bulk metallic glasses, *Prog. Nat. Sci. Mater. Int.*, 20(2011), No.1, p.46.

[20] Y. Zhang, Y.J. Zhou, X.D. Hui, M.L. Wang, and G.L. Chen, Minor alloying behavior in bulk metallic glasses and high-entropy alloys, *Sci. China Ser. G*, 51(2008), No.4, p.427.

[21] S. Wang and Y. Zhang, Shear-band spacing controlled by Bridgman solidification in dendrite/BMG composites, *Sci. China Ser. G*, 52(2009), No.10, p.1632.

[22] J.W. Qiao, Y. Zhang, J.H. Li, and G.L. Chen, Strain rate response of a Zr-based composite fabricated by Bridgman solidification, *Int. J. Miner. Metall. Mater.*, 17(2010), No.2, p.214.

[23] X.C. Zhang, Y. Zhang, X.H. Chen, and G.L. Chen, Bulk metallic glass rings prepared by a modified water quenching method, *Int. J. Miner. Metall. Mater.*, 16(2009), No.1, p.108.

[24] R. H. Yu, The empirical electron theory of solids and molecules, *Chin. Sci. Bull.*, 23(1978), No.4, p.217.